Thermal analysis and Joule-Thomson expansion of black hole exhibiting metric-affine gravity*

Muhammad Yasir[1†]   Tiecheng Xia (夏铁成)[1‡]   Faisal Javed[2,3§]   G. Mustafa[2,4‡]

[1]Department of Mathematics, Shanghai University, Shanghai 200444, China
[2]Department of Physics, Zhejiang Normal University, Jinhua 321004, China
[3]Zhejiang Institute of Photoelectronics and Zhejiang Institute for Advanced Light Source, Zhejiang Normal University, Jinhua 321004, China
[4]New Uzbekistan University, Mustaqillik Ave. 54, Tashkent 100007, Uzbekistan

Abstract: This study examines a recently hypothesized black hole, which is a perfect solution of metric-affine gravity with a positive cosmological constant, and its thermodynamic features as well as the Joule-Thomson expansion. We develop some thermodynamical quantities, such as volume, Gibbs free energy, and heat capacity, using the entropy and Hawking temperature. We also examine the first law of thermodynamics and thermal fluctuations, which might eliminate certain black hole instabilities. In this regard, a phase transition from unstable to stable is conceivable when the first law order corrections are present. In addition, we study the efficiency of this system as a heat engine and the effect of metric-affine gravity for the physical parameters q_e, q_m, κ_s, κ_d, and κ_{sh}. Further, we study the Joule-Thomson coefficient and inversion temperature, and observe the isenthalpic curves in the $T_i - P_i$ plane. In metric-affine gravity, a comparison is made between a van der Waals fluid and a black hole to study their similarities and differences.

Keywords: black hole in metric-affine gravity, thermodynamics, Joule-Thomson expansion

DOI: 10.1088/1674-1137/ad0962

I. INTRODUCTION

The geometrical structure of black holes (BHs) in general relativity (GR) and modified theories of gravity is an attractive and challenging research subject [1]. The thermal characteristics of BHs and their behavior are analyzed by the well-known four laws of BH mechanics [2, 3]. After the study by Bekenstein, for the first time, Stephen Hawking presented the existence of BH radiations and formalized the tunneling process significantly close to the BH horizon owing to the vacuum fluctuations. It was observed that a small quantity of heat led to the eccentricity of quantum mechanics [4, 5]. In [6], it was noted that BHs contain thermodynamic features such as temperature and entropy. At the BH horizon, the Hawking temperature is proportional to its surface gravity because a BH behaves like a thermodynamical system. It was confirmed that the results of [7] are useful for all classical BHs at thermodynamic equilibrium.

The Hawking temperature phase transition occurs after the justification of an isomorphic phase structure associated with the van der Waals liquid-gas system in a Kerr RN-AdS BH [8] and an RN-AdS BH [8, 9]. In all previous BH thermodynamic studies, mass, volume, and pressure, the crucial thermodynamic variables, were missing. The contribution of pressure to this field was completed through the cosmological constant, which also had other basic implications such as the consistency of Smarr's relation with the first law [10]. The cosmological constant (Λ) was taken as the thermodynamic pressure, and the respective first law of thermodynamics was simultaneously modified by the expansion of the phase space with a PdV term, leading to novel understanding of the BH mass [11]. The new perspective on mass with the cosmological constant in BH thermodynamics generated phenomenal consequences in classical thermodynamics. Kubiznak *et al.* [12, 13] presented the AdS BH as a van der Waals system and investigated the critical behavior of

the BH through the $P - v$ isotherm, Gibbs free energy, critical exponents, and coincidence curves, which are all presented as similar to the van der Waals case. Moreover, these similar features were obtained on various AdS BHs in [14−19]. The similarities to classical thermodynamics, such as holographic heat engines [20], Joule Thomson expansion, phase transitions, and Clausius-Clapeyron equation, were also studied in [21, 22]. Javed *et al.* [23] investigated the thermodynamics of charged and uncharged BHs in symmetric teleparallel gravity. They also studied the thermal fluctuations and phase transition of the considered BHs. The dynamical configurations of thin-shell developed from BHs in metric- affine gravity composed with scalar field were studied in [24]. Some interesting physical characteristics of various BH solutions were dicussed in [25−26].

In addition, the Joule-Thomson expansion was investigated in AdS BHs by Ökcü and Aydiner [27], further proceeding to the isenthalpic process by which gas expands through a porous plug from a high-pressure section to a low-pressure section. The researchers also analyzed the Joule-Thomson expansion phenomenon in Kerr-AdS BHs within the extended phase space [28]. They examined both the isenthalpic and numerical inversion curves in the temperature-pressure plane, illustrating regions of cooling and heating for Kerr-AdS BHs. Additionally, they computed the ratio between the minimum inversion temperature and critical temperature for Kerr-AdS BHs [28]. This pioneering work was generalized to quintessence holographic superfluids of RN BHs in $f(R)$ gravity [29−31]. More recently, we studied, in detail, the consequence of the dimensionality on the Joule-Thomson expansion in [31]. As stated in [31, 32], the ratio between the critical temperature and minimum inversion temperature decreases with the dimensionality d, while it retrieves the results when $d = 4$. In this work, we investigated whether the existence of metric-affine gravity should influence the Joule-Thomson expansion, which is also motivated by the progress in our understanding of metric-affine gravity. Here, we propose that the adopted strategy is contextualized not only for BHs in metric-affine gravity but also for those in other alternative theories of gravity where new gravitational modes are well developed.

This paper is devoted to explore the effects of metric-affine gravity on the phase transition of BH geometry and also to study the Joule-Thomson expansion. The remaining of this paper is arranged as follows. In Sec. II, we present a brief review of our new class of BHs in metric-affine gravity. In Sec. III, we formulate the thermodynamic quantities, such as temperature, pressure, Gibbs free energy, and heat engine. Next, in Sec. IV, we introduce the Joule-Thomson expansion for a classical physical quantity. Finally, we present a few closing remarks.

II. A BRIEF REVIEW ON BLACK HOLES IN METRIC-AFFINE GRAVITY

GR is the most successful and physically acceptable theory of gravity, which precisely describes the gravitational interaction in the space-time geometry and the characteristics of matter via the energy-momentum tensor. From a geometrical perspective, the Lorentzian metric tensor $g_{\mu\nu}$ is considered to study the smooth manifold that is used to develop the Levi-Civita affine connection $\Gamma^\lambda_{\mu\nu}$. To establish a model where the largest family of BH solutions with dynamical torsion and nonmetricity in metric-affine gravity can be found, a propagating traceless nonmetricity tensor must be taken into account in the gravitational action of metric-affine gravity. As a geometrical correction to GR, a quadratic parity-preserving action presenting a dynamical traceless nonmetricity tensor in this situation is given as follows [33−37]:

$$
S = \int \mathrm{d}^4 x \sqrt{-g} \left\{ \mathcal{L}_\mathrm{m} + \frac{1}{16\pi} \left[- R + 2f_1 \tilde{R}_{(\lambda\rho)\mu\nu} \tilde{R}^{(\lambda\rho)\mu\nu} \right. \right.
$$
$$
\left. \left. + 2f_2 \left(\tilde{R}_{(\mu\nu)} - \hat{R}_{(\mu\nu)} \right) \left(\tilde{R}^{(\mu\nu)} - \hat{R}^{(\mu\nu)} \right) \right] \right\}, \tag{1}
$$

where $\tilde{R}^{(\lambda\rho)\mu\nu}$ and $\tilde{R}_{(\mu\nu)}$ are the affine-connected form of Riemann and Ricci tensors. Here, R denotes the Ricci scalar, g is the determinant of the metric tensor, $\mathcal{L}_m$ depicts the matter Lagrangian, and f_1, f_2 are Lagrangian coefficients. This solution can also be easily generalized to take into account the cosmological constant and Coulomb electromagnetic fields with electric charge (q_e) and magnetic charge (q_m), which are decoupled from torsion [38, 39]. This assumes the minimal coupling principle.

$$
\tilde{R}^{(\lambda\rho)}_{\mu\nu} = \frac{1}{2} T^\sigma_{\mu\nu} Q^{\lambda\rho}_\sigma + \tilde{\nabla}_{[\nu} Q^{\lambda\rho}_{\mu]},
$$
$$
\tilde{R}_{(\mu\nu)} - \hat{R}_{(\mu\nu)} = \tilde{\nabla}_{(\mu} Q^\lambda_{\nu)\lambda} + Q_{\lambda\rho(\mu} Q^{\lambda\rho}_{\nu)}
$$
$$
- \tilde{\nabla}_\lambda Q^\lambda_{(\mu\nu)} - Q^{\lambda\rho}_{\lambda} Q_{(\mu\nu)\rho} + T_{\lambda\rho(\mu} Q^{\lambda\rho}_{\nu)\rho}, \tag{2}
$$

These variations represent the third Bianchi of GR. By executing changes of the above equations with respect to the co-frame field and the anholonomic interrelation, the following field equations are established: $Y1^\nu_\mu = 8\pi\theta^\nu_\mu$ and $Y2^{\lambda\mu\nu} = 4\pi\Delta^{\lambda\mu\nu}$, where $Y1_\mu{}^\nu$ and $Y2^{\lambda\mu\nu}$ are tensor quantities. $\Delta^{\lambda\mu\nu}$ and $\theta_\mu{}^\nu$ are utilized to study the hyper momentum density and canonical energy-momentum tensors of matter, which are expressed as

$$
\Delta^{\lambda\mu\nu} = \frac{\mathrm{e}^{a\lambda} e_b{}^\mu}{\sqrt{-g}} \frac{\delta \left(\mathcal{L}_m \sqrt{-g} \right)}{\delta\omega^a{}_{b\nu}},
$$
$$
\theta_\mu{}^\nu = \frac{\mathrm{e}^a{}_\mu}{\sqrt{-g}} \frac{\delta \left(\mathcal{L}_m \sqrt{-g} \right)}{\delta\mathrm{e}^a{}_\nu}. \tag{3}
$$

Therefore, both matter representations act as sources of the extended gravitational field. In this scenario, metric-affine geometries utilize the Lie algebra of the general linear group GL(4, R) in anholonomic interrelation. This hypermomentum presents its proper decomposition into shear, spin, and dilation currents [36, 37]. Furthermore, the effective gravitational action of the model is provided in terms of these properties. The parameterizations of the spherically symmetric static spacetime are as follows: [39−43]

$$ds^2 = -\Psi(r)dt^2 + \Psi^{-1}(r)dr^2 + r^2d\theta^2 + r^2\sin^2\theta d\phi^2. \quad (4)$$

Compared with the standard case of GR, in the emission process, a matter current coupled to torsion and nonmetricity in a general splitting of the energy levels will potentially affect this spectrum and the efficiency. Interestingly, the performance of a perturbative interpretation on the energy-momentum tensor in vacuum fluctuations of the quantum field coupled to the torsion, as well as nonmetricity tensors of the solution, is used to study the rate of dissipation obtained on its event horizon, which would also cover the further corrections with respect to the system of GR [44, 45]. The metric function (Reissner-Nordström-de Sitter-like) is defined as [37]

$$\Psi(r) = 1 - \frac{2m}{r} + \frac{d_1\kappa_s^2 - 4e_1\kappa_d^2 - 2f_1\kappa_{sh}^2 + q_e^2 + q_m^2}{r^2} + \frac{\Lambda}{3}r^2, \quad (5)$$

which represents the broadest family-charged BH models obtained in metric-affine gravity with real constants e_1 and d_1. Here, κ_{sh}, κ_s, and κ_d represent the shear, spin, and dilation charges, respectively.

III.   THERMODYNAMICS

A cosmological constant is treated as a thermodynamic variable. After the thermodynamic pressure of the BH is put into the laws of thermodynamics, the cosmological constant is considered as the pressure. From the equation of horizon $\Psi(r) = 0$ and pressure $P = -\frac{\Lambda}{8\pi}$ [29, 30], we can deduce the relation between the BH mass m and its event horizon radius, r_h, which is expressed as follows

$$m = \frac{3d_1\kappa_s^2 - 6f_1\kappa_{sh}^2 - 8\pi Pr_h^4 + 3q_e^2 + 3q_m^2 + 3r_h^2 - 12\kappa_d^2 e_1}{6r_h}. \quad (6)$$

The Hawking temperature of the BH related to surface gravity can be obtained as

$$T = \frac{\Psi'(r)}{4\pi} = \frac{6 - 32\pi Pr_h^2}{12\pi r_h}$$
$$- \frac{3d_1\kappa_s^2 - 6f\kappa_{sh}^2 - 8\pi Pr_h^4 + 3q_e^2 + 3q_m^2 + 3r_h^2 - 12\kappa_d^2 e_1}{12\pi r_h^3}. \quad (7)$$

It has a peak as shown in Figs. 1 and 2 and shifts to right (positive) and increases with increasing P_c and κ_s. The temperature becomes the absence of the electric charge ($q = 0$). As we increase the values of P_c and κ_s, the local maximum of the Hawking temperature increases, as exhibited in Figs. 1 and 2. Further, the temperature converges when the horizon radius shrinks to zero for the considered BH manifold. The general form of the first law of BH thermodynamics can be written as [29−32, 46, 47]

$$dM = TdS + VdP + \Phi dq_m + \varphi dq_e + \Bbbk_{sh}d\kappa_{sh}$$
$$+ \Bbbk_s d\kappa_s + \Bbbk_d d\kappa_d + E1de_1 + F_1df_1 + D_1dd_1, \quad (8)$$

where M, S, V, P, Q, Φ, and φ are the mass, entropy, volume, pressure, magnetic charge, and chemical potential of BH, respectively. They have been treated as thethermodynamic variables corresponding to the conjugating variables $\Bbbk_{sh}$, $\Bbbk_s$, $\Bbbk_d$, $E1$, and d_1, respectively. The volume and chemical potential of the BH are defined as

$$V = \left(\frac{\partial M}{\partial P}\right)_{S,q_m}, \quad \Phi = \left(\frac{\partial M}{\partial q_m}\right)_{S,P}, \quad (9)$$

respectively. The BH entropy with the help of area is defined as [48−50]

$$S = \frac{A}{4} = \pi r_h^2. \quad (10)$$

From Eqs. (6) and (7), the equation of state for the BH can easily be expressed as

$$P = -\frac{d_1\kappa_s^2 - 2f_1\kappa_{sh}^2 + q_e^2 + q_m^2 + 4\pi r_h^3 T - r_h^2 - 4\kappa_d^2 e_1}{8\pi r_h^4}. \quad (11)$$

The red, blue, orange, and black colors indicate the divergence at pressures below the critical pressure. The oscillations of the isotherms at critical temperatures in the $P - v_h$ diagram are equivalent to the unstable BHs that are presented by negative heat capacity in this section (Figs. 3 and 4). These divergences are the characteristics of the first-order phase transition that occurs between smaller and larger BHs that are stable and have a positive heat capacity. In response to changes in the value of the parameter T_c, there is a corresponding shift in the horizontal axis; an increase in this parameter results in a reduction in the critical radius.

The thermodynamic variables V, Φ, φ and the conjugating quantities $\Bbbk_{sh}$, $\Bbbk_s$, $\Bbbk_d$, $E1$, and d_1 are obtained from the first law as
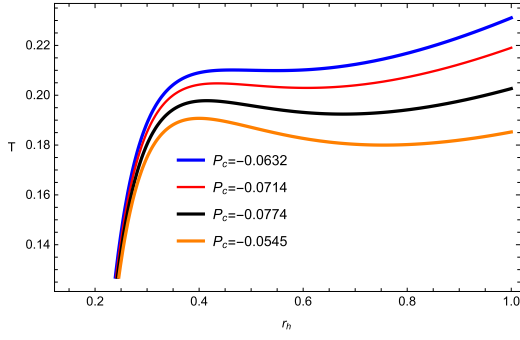
Fig. 1. (color online) Plot of temperature T with fixed $q_e = 0.28$; $q_m = 0.08$; $d_1 = 0.004$; $f_1 = 0.313$; $\kappa_d = 0.02$; $\kappa_s = 0.8$; and $e_1 = 0.4$.
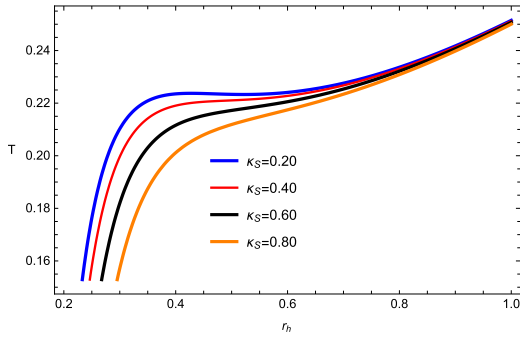
Fig. 2. (color online) Plot of temperature T with fixed $q_e = 0.28$; $q_m = 0.08$; $d_1 = 0.004$; $f_1 = 0.313$; $\kappa_d = 0.02$; and $e_1 = 0.4$.

$$V = \frac{4\pi r_h^3}{3}, \quad \Phi = \frac{q_m}{r}, \quad \varphi = \frac{q_e}{r},$$

$$\Bbbk_{\text{sh}} = \frac{-2f_1\kappa_{\text{sh}}}{r}, \quad \Bbbk_s = \frac{d_1\kappa_s}{r}, \quad \Bbbk_d = \frac{-4e_1\kappa_d}{r},$$

$$E1 = \frac{-4\kappa_d^2}{r} \text{ and } D_1 = \frac{\kappa_s^2}{r}. \tag{12}$$

A. Gibbs free energy and specific heat

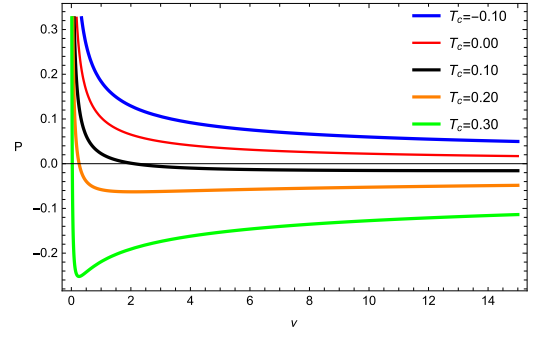The most important and basic thermodynamic quant-

Fig. 3. (color online) Plot of temperature P with fixed $q_m = 0.0002$; $d_1 = 0.004$; $f_1 = 0.003$; $\kappa_d = 0.01$; $\kappa_s = 0.03$; and $e_1 = 0.4$.

Fig. 4. (color online) Plot of temperature P with fixed $q_m = 0.0002$; $d_1 = 0.004$; $f_1 = 0.003$; $\kappa_d = 0.01$; $\kappa_s = 0.03$; and $e_1 = 0.4$.

ity is the Gibbs free energy of a BH, which can be utilized to explore the small/larger BH phase transition by studying the $G - r_h$ and $G - T$ diagrams. In addition, the Gibbs free energy also helps us to investigate the global stability of a BH. It can be evaluated as [51, 52]

$$G = -TS + M. \tag{13}$$

Using Eqs. (6) and (7) in (13), we obtain

$$G = \frac{\sqrt[3]{\frac{\pi}{6}}\left(12d_1\kappa_s^2 - 24f\kappa_{\text{sh}}^2 + 4\sqrt[3]{\frac{6}{\pi}}Pv^{4/3} + 12q_e^2 + 12q_m^2 + \left(\frac{6}{\pi}\right)^{2/3}v^{2/3} - 48\kappa_d^2 e_1\right)}{8\sqrt[3]{v}}. \tag{14}$$
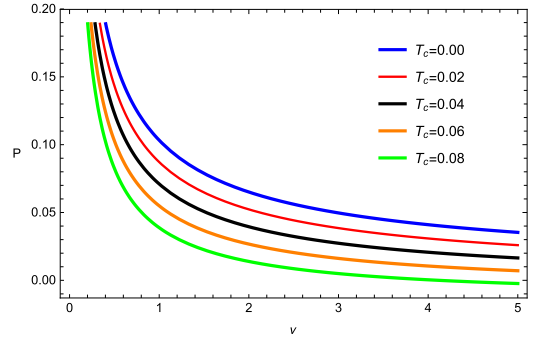
We observe the graphical behavior of the phase transitions in the $G - r_h$ plane as shown in Figs. 5 and 6. It is noted that the Gibbs free energy decreases as the critical radius increases. To calculate the critical thermodynamic properties of a BH, one can use the following condition:

$$\left(\frac{\partial P}{\partial v_h}\right)_T = \left(\frac{\partial^2 P}{\partial v_h^2}\right)_T = 0. \tag{15}$$

Using Eq. (15), the critical temperature can be expressed as

$$T_c = \frac{1}{3\sqrt{6\pi}\sqrt{d_1\kappa_s^2 - 2f_1\kappa_{\text{sh}}^2 + q_e^2 + q_m^2 - 4\kappa_d^2 e_1}}. \tag{16}$$
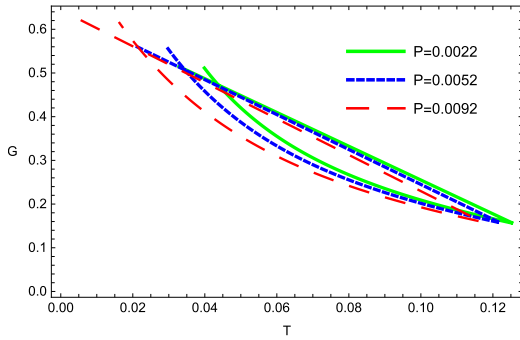
From Eq. (15), the critical radius of BH is as follows:

$$v_c = 8\sqrt{6\pi}\left(d_1\kappa_s^2 - 2f_1\kappa_{\text{sh}}^2 + q_e^2 + q_m^2 - 4\kappa_d^2 e_1\right)^{3/2}. \tag{17}$$

The critical pressure in terms of other parameters takes the following form:
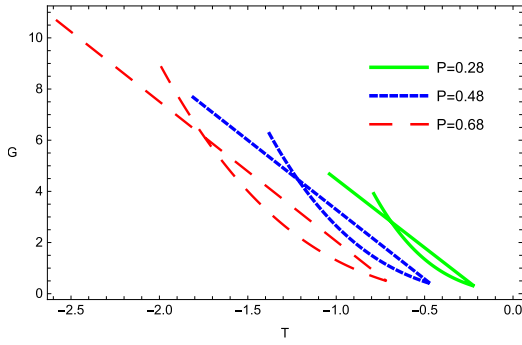
Fig. 5. (color online) Plot of Gibbs free energy G with fixed $q_m = 0.003$; $d_1 = 0.200$; $f_1 = 0.050$; $\kappa_d = 0.010$; and $e_1 = 0.050$.

Fig. 6. (color online) Plot of Gibbs free energy G with fixed $q_m = 0.003$; $d_1 = 0.200$; $f_1 = 0.050$; $\kappa_d = 0.010$; and $e_1 = 0.050$.

$$P_c = \frac{1}{96\pi \left(-d_1\kappa_s^2 + 2f_1\kappa_{sh}^2 - q_e^2 - q_m^2 + 4\kappa_d^2 e_1\right)^2}. \tag{18}$$

However, we applied a numerical analysis because calculating the critical numbers analytically is not a simple operation.

To find more data about a phase transition, we studied a thermodynamic quantity such as heat capacity. By applying the standard definition of heat capacity as follows: [46, 53]

$$C_p = T\left(\frac{\partial S}{\partial T}\right)_P, \tag{19}$$

with a few numerical calculations, one can obtain a dimensionless important relation for the amounts P_c, T_c, and v_c. If the expression $(d_1\kappa_s^2 - 2f_1\kappa_{sh}^2 + q_e^2 + q_m^2 - 4\kappa_d^2 e_1) \to$ 1.327765310 is provided, then our solution satisfies the well-known condition as

$$\frac{P_c v_c}{T_c} = 3/8, \tag{20}$$

and similar results are studied in the context of the van der Waals equation and in an RN-AdS BH . Therefore, the negative heat capacity that gives the temperamental (unstable) BH is also related to the critical temperature in the $P - v_h$ plane. The expressions of volume and entropy of a BH are presented in Eqs. (7) and (10). From Eq. (19), we obtain

$$C_p = \frac{3^{2/3}\sqrt[3]{\frac{\pi}{2}}v^{2/3}\left(4d\kappa_s^2 - 8f\kappa_{sh}^2 + 12\sqrt[3]{\frac{6}{\pi}}Pv^{4/3} + 4q_e^2 + 4q_m^2 - \left(\frac{6}{\pi}\right)^{2/3}v^{2/3} - 16\kappa_d^2 e_1\right)}{-12d\kappa_s^2 + 24f\kappa_{sh}^2 + 12\sqrt[3]{\frac{6}{\pi}}Pv^{4/3} - 12q_e^2 - 12q_m^2 + \left(\frac{6}{\pi}\right)^{2/3}v^{2/3} + 48\kappa_d^2 e_1}. \tag{21}$$

It has been discovered that the critical amounts classify the behavior of thermodynamic quantities close to the critical point. In Figs. 7 and 8, for thermodynamically stable BHs, we separate the two cases in which the heat capacity is positive ($r_h < r_c$) and the case in which it is negative ($r_h > r_c$). The second-order phase transition is implied by the instability areas of BHs, where the heat capacity is discontinuous at the critical temperature $r_h = r_c$ [54, 55]. It is noted that the heat capacity diverges at $r_h = 0.50$, when T_h reaches its maximum value as

$T_h = 0.24$ for $r_h = 1.00$, $q_m = 0.08$, $d_1 = 0.004$, $f_1 = 0.313$, $\kappa_d = 0.02$, and $e_1 = 0.4$. The critical points in the alternate phase space are obtained by utilizing the standard definition, and we reduced the thermodynamic variables as follows:
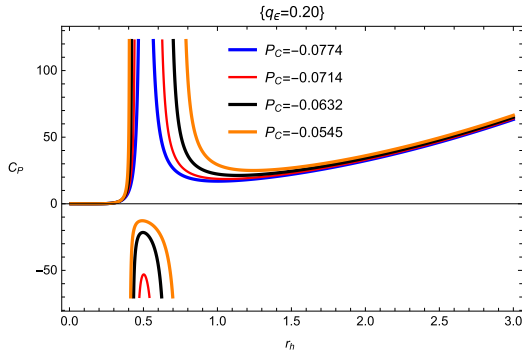
$$T_r = \frac{T}{T_c}, \quad v_r = \frac{v}{v_c} \quad \text{and} \quad P_r = \frac{P}{P_c}. \tag{22}$$
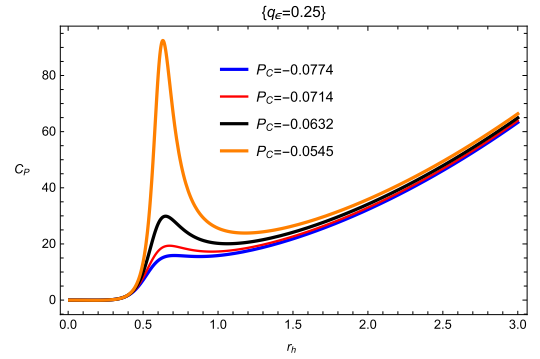
The reduced variables can be written as

$$T_r = -\frac{3\sqrt{\frac{3}{2}}\sqrt{d_1\kappa_s^2 - 2f\kappa_{sh}^2 + q_e^2 + q_m^2 - 4\kappa_d^2 e_1}\left(d_1\kappa_s^2 - 2f_1\kappa_{sh}^2 + 8\pi Pr_h^4 + q_e^2 + q_m^2 - r_h^2 - 4\kappa_d^2 e_1\right)}{2r_h^3}, \tag{23}$$

volume can be obtained as

Fig. 7.   (color online) Plot of heat capacity with fixed $q_m = 0.08$; $d_1 = 0.004$; $f_1 = 0.313$; $\kappa_d = 0.02$; and $e_1 = 0.4$.

Fig. 8.   (color online) Plot of heat capacity with fixed $q_m = 0.08$; $d_1 = 0.004$; $f_1 = 0.313$; $\kappa_d = 0.02$; and $e_1 = 0.4$.

$$v_r = \frac{r^3}{6\sqrt{6}\left(d_1\kappa_s^2 - 2f_1\kappa_{\mathrm{sh}}^2 + q_e^2 + q_m^2 - 4\kappa_d^2 e_1\right)^{3/2}}, \tag{24}$$

and pressure is as follows:

$$P_r = -\frac{12\left(d_1\kappa_s^2 - 2f_1\kappa_{\mathrm{sh}}^2 + q_e^2 + q_m^2 - 4\kappa_d^2 e_1\right)^2 \left(d_1\kappa_s^2 - 2f_1\kappa_{\mathrm{sh}}^2 + q_e^2 + q_m^2 + 4\pi r_h^3 T - r_h^2 - 4\kappa_d^2 e_1\right)}{r_h^4}. \tag{25}$$

Two adiabatic and two isothermal processes combined to form the Carnot cycle are the hallmark of the most effective heat engine. The single most fundamental and critical feature of the Carnot cycle is that the heat engine efficiency is a function of reservoir temperatures:

$$\eta = 1 - \frac{T_c}{T_h}, \tag{26}$$

and as a reservoir can never be at zero temperature, the efficiency cannot be one because T_c and T_h denote cold and hot reservoirs, respectively. Hence, we obtain

$$\eta = 1 + \frac{2\sqrt{\frac{2}{3}}r_h^3}{3\sqrt{d_1\kappa_s^2 - 2f_1\kappa_{\mathrm{sh}}^2 + q_e^2 + q_m^2 - 4\kappa_d^2 e_1}\left(d\kappa_s^2 - 2f_1\kappa_{\mathrm{sh}}^2 + 8\pi P r_h^4 + q_e^2 + q_m^2 - r_h^2 - 4\kappa_d^2 e_1\right)}. \tag{27}$$

Now, we study the behavior of the heat engine efficiency η as a function of the the pressure P and entropy S matching to the heat cycle provided in Figs. 9 and 10, for the different values of metric-affine gravity parameters. From these figures, we can observe that the nature of the heat engine efficiency is essentially relying on the metric-affine gravity parameters. In addition, for a given set of input values, the efficiency of the heat engine increases monotonically as the horizon's radius grows. Because of this, larger BHs should expect higher heat-engine efficiency. In other words, they allow for a maximum efficiency curve to be provided for a heat engine by varying only a few fixed parameters (the BH works at the highest efficiency). Here, the local stability is related to the system, but it can be large with small changes in the values of thermodynamic parameters. Thus, the term heat capa-

city gives information on local stability. In [36], it is stated how the cosmological constant Λ can be studied by treating it as a scale parameter.

IV. JOULE-THOMSON EXPANSION

One of the best-known and classical physical processes to explain the change in temperature of a gas flowing from a high-pressure to a reduced pressure section through a porous plug is called the Joule-Thomson expansion. The main focus is on the gas expansion process, which expresses the cooling effect (when the temperature drops) and the heating effect (when the temperature increases), with the enthalpy remaining constant throughout the process. This change depends upon the Joule-Thomson coefficient: [28, 56]
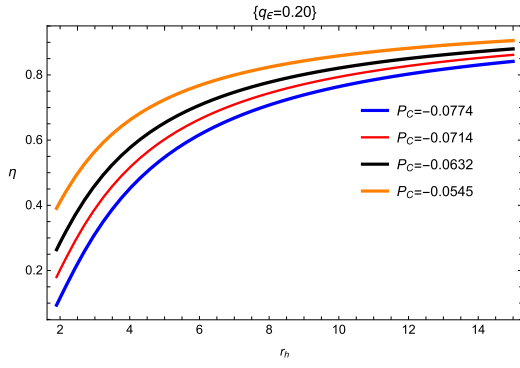
Fig. 9. (color online) Plot of efficiency η with fixed $q_m = 0.08$; $d_1 = 0.004$; $f_1 = 0.313$; $\kappa_d = 0.02$; and $e_1 = 0.4$.
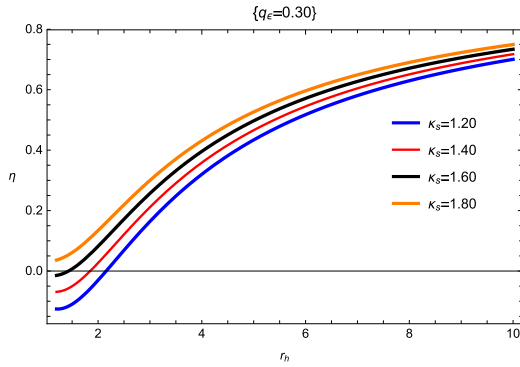
Fig. 10. (color online) Plot of efficiency η with fixed $q_m = 0.08$; $d_1 = 0.004$; $f_1 = 0.313$; $\kappa_d = 0.02$; and $e_1 = 0.4$.

$$\mu_{JT} = \left(\frac{\partial T}{\partial P}\right)_H = \frac{1}{C_p}\left[T\left(\frac{\partial V}{\partial T}\right)_p - V\right]. \quad (28)$$

Using Eqs. (7), (9), (21), and (28), the coefficient is calculated as follows:

$$\mu_{JT} = \frac{4r_h\left(3d_1\kappa_s^2 - 6f_1\kappa_{sh}^2 + 8\pi Pr_h^4 + 3q_e^2 + 3q_m^2 - 2r_h^2 - 12\kappa_d^2 e_1\right)}{3\left(d_1\kappa_s^2 - 2f\kappa_{sh}^2 + 8\pi Pr_h^4 + q_e^2 + q_m^2 - r_h^2 - 4\kappa_d^2 e_1\right)}. \quad (29)$$

The study of the Joule-Thomson coefficient versus the horizon r_h is shown in Figs. 11, 12, 13, and 14. We set $d_1 = 0.004$, $f_1 = 0.313$, $\kappa_{sh} = 0.05$, $\kappa_d = 0.02$, $\kappa_s = 0.8$, and $e_1 = 0.4$ in that order. There exist both divergence points and zero points for different variations of κ_d, κ_s, and κ_{sh} respectively. It is clear from a comparison of these figures that the zero point of the Hawking temperature and the divergence point of the Joule-Thomson coefficient is the same. This point of divergence gives information on the Hawking temperature and corresponds to the most extreme BHs. From Eq. (29) and utilizing the well-known condition $\mu_{JT} = 0$, the temperature inversion occurs as
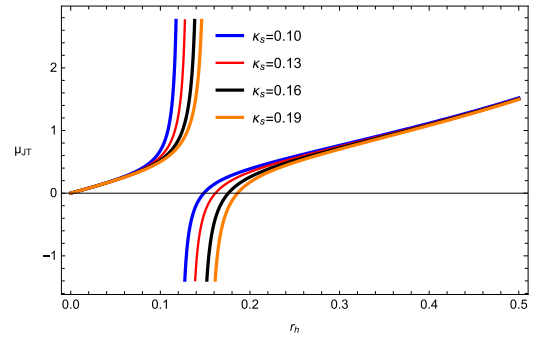
$$T_i = \frac{3d_1\kappa_s^2 - 6f_1\kappa_{sh}^2 - 8\pi Pr_h^4 + 3q_e^2 + 3q_m^2 - r_h^2 - 12\kappa_d^2 e_1}{12\pi r_h^3}. \quad (30)$$
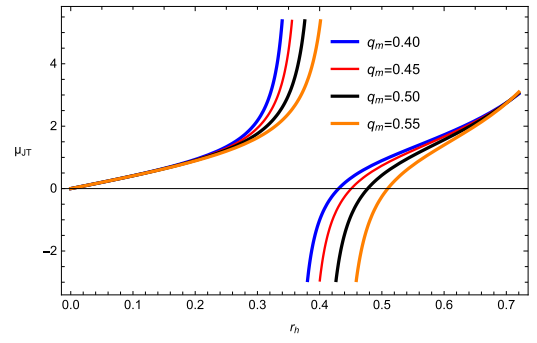
Fig. 11. (color online) Joule-Thomson coefficient μ_{JT} plane with fixed $d_1 = 0.03$; $f_1 = 0.01$; $\kappa_d = 0.02$; $\kappa_s = 0.10$; and $e_1 = 0.04$.
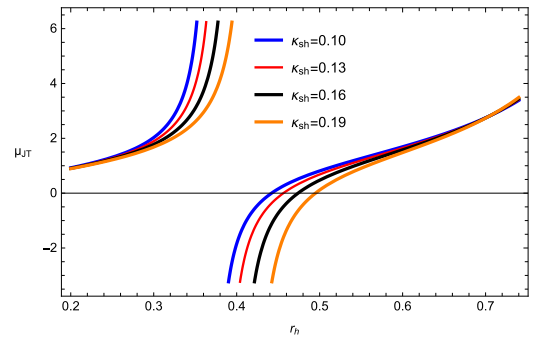
Fig. 12. (color online) Joule-Thomson coefficient μ_{JT} with fixed $d_1 = 0.03$; $f_1 = 0.01$; $\kappa_d = 0.02$; $\kappa_s = 0.10$; and $e_1 = 0.04$.


Fig. 13. (color online) Joule-Thomson coefficient μ_{JT} with fixed $d_1 = 0.03$; $f_1 = 0.01$; $\kappa_{sh} = 0.10$; $\kappa_d = 0.02$; and $e_1 = 0.04$.

Because the Joule-Thomson expansion is an isenthalpic process, it is important to analyze the isenthalpic curves of BHs under metric-affine gravity, which are depicted in Figs. 15−18. Thus, we study the isenthalpic curves ($T_i - P_i$ plane) by assuming different values of BH mass, which are investigated in Eq. (29) with a larger root of r_h. We show the isenthalpic and inversion curves of BHs in metric-affine gravity and the result is consistent [57−60]. The heating and cooling zones are characterized by the inversion curve, and the isenthalpic curves possess positive slopes above the inversion curve. In contrast, the pressure always falls in a Joule-Thomson expansion and the slope changes sign when heating occurs below the inver-

Fig. 14. (color online) Joule-Thomson coefficient μ_{JT} with fixed $d_1 = 0.03$; $f_1 = 0.01$; $\kappa_{\mathrm{sh}} = 0.10$; $\kappa_s = 0.10$; and $e_1 = 0.04$.
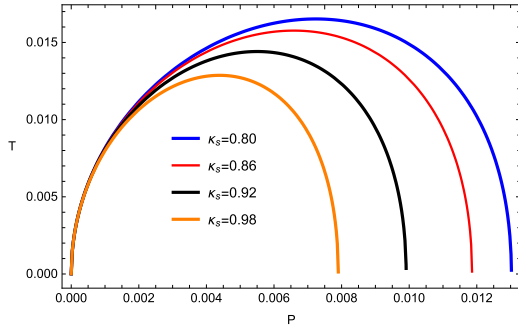
Fig. 15. (color online) Isenthalpic curves $(T - P)$ plane with fixed $d_1 = 0.004$; $f_1 = 0.313$; $\kappa_{\mathrm{sh}} = 0.05$; $\kappa_d = 0.02$; and $e_1 = 0.4$.
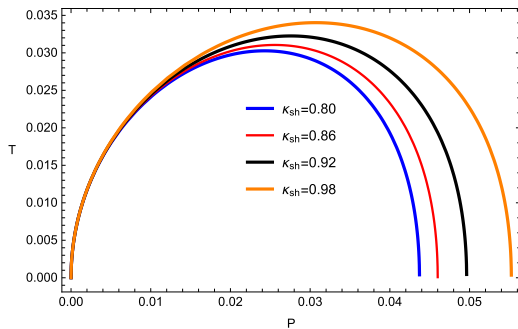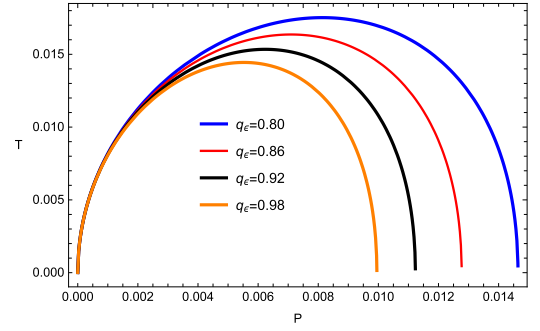

Fig. 16. (color online) Isenthalpic curves $(T - P)$ plane with fixed $d_1 = 0.004$; $f_1 = 0.313$; $\kappa_d = 0.02$; $\kappa_s = 0.8$, and $e_1 = 0.4$.

sion curve. The heating process appears at higher temperatures, as indicated by the negative slope of the constant mass curves in the Joule-Thomson expansion. When temperatures drop, cooling begins, which is linked to the positive slope of the constant mass curves. From above equation, one can deduce the inversion pressure as

$$P_i = \frac{3d_1\kappa_s^2 - 6f_1\kappa_{\mathrm{sh}}^2 + 3q_e^2 + 3q_m^2 - 12\pi r_h^3 Ti - r_h^2 - 12\kappa_d^2 e_1}{8\pi r_h^4}.$$
(31)

The inversion curves for different values, $d_1 = 0.004$, $f_1 = 0.313$, $\kappa_{\mathrm{sh}} = 0.05$, and $\kappa_d = 0.02$, are shown in Figs. 19, 20, 21, and 22. The inversion temperature increases with variations of the important parameters m, q_e, κ_{sh}, and

Fig. 17. (color online) Isenthalpic curves $(T - P)$ plane with fixed $d_1 = 0.004$; $f_1 = 0.313$; $\kappa_{\mathrm{sh}} = 0.05$; $\kappa_d = 0.02$; $\kappa_s = 0.8$, and $e_1 = 0.4$.
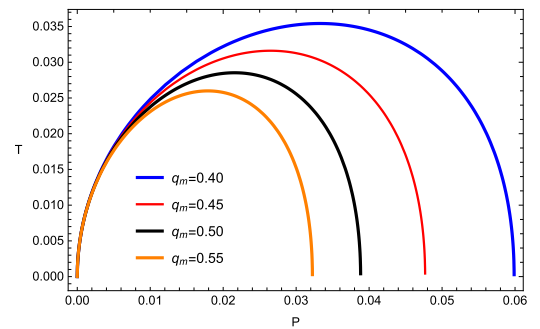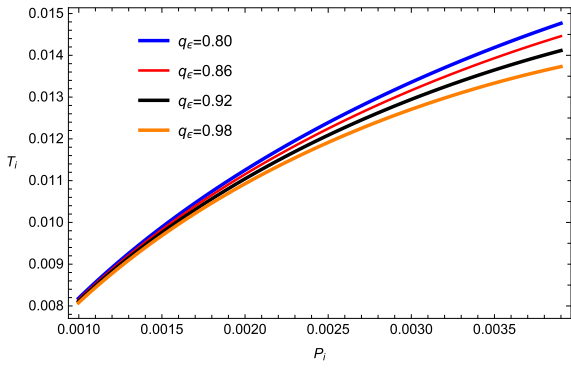

Fig. 18. (color online) Isenthalpic curves $T - P$ plane with fixed $d_1 = 0.004$; $f_1 = 0.313$; $\kappa_{\mathrm{sh}} = 0.05$; $\kappa_d = 0.02$; $\kappa_s = 0.8$; and $e_1 = 0.4$.
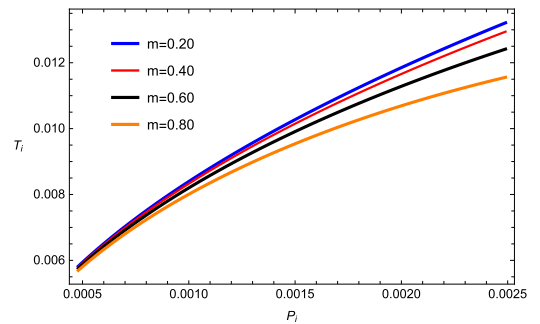
Fig. 19. (color online) Inversion curves $(Ti - Pi)$ with fixed $d_1 = 0.004$; $f_1 = 0.313$; $\kappa_{\mathrm{sh}} = 0.05$; $\kappa_d = 0.02$; $\kappa_s = 0.8$; and $e_1 = 0.4$.

κ_s, respectively. We can go back to the case of the BH in metric-affine gravity. Compared with the van der Waals fluids, we can observe from Figs. 19−22 that the inversion curve is not closed. From the above results, in the $Ti - Pi$ plane at low pressure, the inversion temperature T_i decreases with the increase in charge q_e and mass m, and it shows the opposite behavior for higher pressure. It is also clear that, unlike the case with van der Waals fluids, the inversion temperature continues to rise monotonically with increasing inversion pressure, and hence, the inversion curves are not closed [59, 60].
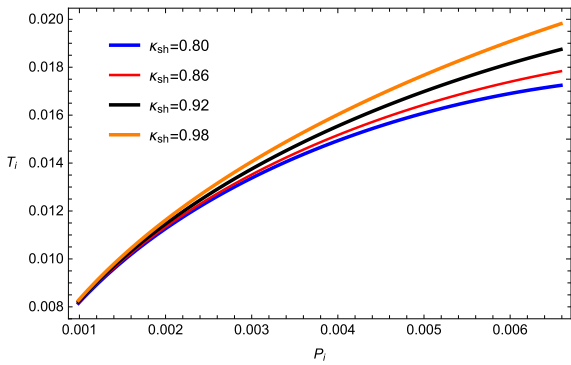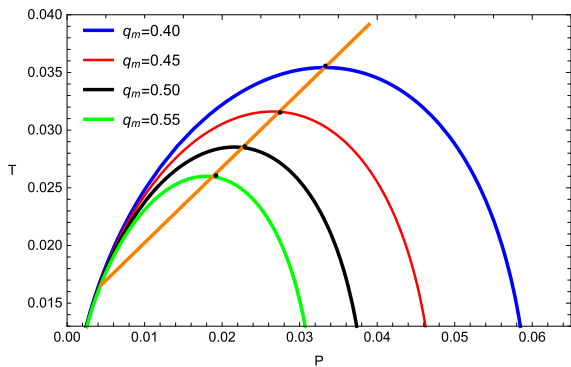
Fig. 20. (color online) Inversion curves ($Ti - Pi$) with fixed $d_1 = 0.004$; $f_1 = 0.313$; $\kappa_{sh} = 0.05$; $\kappa_d = 0.02$; $\kappa_s = 0.8$; and $e_1 = 0.4$.

Fig. 21. (color online) Inversion curves ($Ti - Pi$) plane with fixed $d_1 = 0.004$; $f_1 = 0.313$; $\kappa_d = 0.02$; $\kappa_s = 0.8$; and $e_1 = 0.4$.

Fig. 22. (color online) Inversion curves ($Ti - Pi$) plane with fixed $d_1 = 0.004$; $f_1 = 0.313$; $\kappa_{sh} = 0.05$; $\kappa_d = 0.02$; and $e_1 = 0.4$.

V. CONCLUSION

In this work, we considered a BH in metric-affine gravity, studied the thermodynamics in the presence of Bekinstien entropy, and examined the standard thermodynamics relations. In detail, we thoroughly investigated the thermodynamics to analytically obtain thermodynamical properties such as the Hawking temperature, entropy, specific heat, and free energy associated with BHs in metric-affine gravity with a focus on the stability of the system. The heat capacity blows at r_c, which is a double

horizon, and local maxima of the Hawking temperature also occur at r_c. It is shown that the heat capacity is positive for $r_h < r_c$, providing stability to small BHs close to perturbations in the region, and at a critical radius a phase transition exists. The BH is unstable for $r_h > r_c$ with negative heat capacity. The global analysis of the stability of BHs is also discussed by calculating the free energy G_h. For negative free energy $G_h < 0$ and positive heat capacity $C_p > 0$, it is noted that smaller BHs are globally stable, and these results are also used in [14−19]. We calculated the inverse temperature, inverse pressure, and mass parameter, and investigated the Joule-Thomson process of the system. The negative cosmological constant in metric-affine gravity was investigated for phase transitions of BHs. Above the inversion curves, we examined the cooling region, whereas below the inversion curve there is a heating one. The corresponding results can be summarized as follows: both the inversion temperature and pressure become greater with an increasing BH in metric-affine gravity while they decrease with the charge q_e. The physical consequences are analogous to those in holography; a BH would be a system as well as dual to conformal field theories. The BH in metric-affine gravity is studied and its thermodynamics is identical to that of usual systems; the thermodynamical analysis becomes more complete. Our results show that the Joule-Thomson coefficient is independent of the shear, spin, and dilation charges, which indicates that the Joule-Thomson expansion considered here is universal. In particular, we find novel isenthalpic curves in which the inversion temperature of the Joule-Thomson expansion, rather than the extreme one reported by previous works, separates heating and cooling phases [61−63]. Therefore, our inversion curves separate the allowable and forbidden regions for the Joule-Thomson effect to be observed, where the Joule-Thomson coefficient is the essential quantity to discriminate between the cooling and heating regimes of the system. It is worth noting that when a thermal system is amplified with a temperature, the pressure always decreases yielding a negative sign to ∂P.

Our analysis of inversion curves in the plane revealed that the influence of the parameters on a BH may be more evident in space-time. We analyzed the BH in metric-affine gravity and the characteristics of the inversion curve; these included the shear, spin, and dilation charges. In these figures, we observed that the inversion curves are compatible with the extreme point of a specific isenthalpic curve, and the cooling as well as heating regions are identified. In other words, the boundary between the heating-cooling regions of the BH in metric-affine gravity influences the inversion curves. We also discovered the maximum expansion points of the cooling-heating regimes, as in [64−66]. For the BH heat engine, we investigated the analytical expression for efficiency in terms of horizon radius, pressures, and temperatures in

various limits. We also studied the Joule-Thomson expansion, isenthalpic curves, and inversion curves of the considered BH in metric affine gravity, as follows:

● We examined the Joule-Thomson expansion for a BH in metric-affine gravity, where the cosmological constant is taken as a pressure. We mainly focused on the BH mass considered enthalpy, which is the mass that does not change during the expansion. The Joule-Thomson coefficient μ_{JT} in terms of horizon r_h is shown in Figs. 11−14. There exist both divergence points and zero points with $d_1 = 0.004$, $f_1 = 0.313$, $\kappa_{sh} = 0.05$, $\kappa_d = 0.02$, $\kappa_s = 0.8$, and $e_1 = 0.4$. The zero point of the Hawking temperature, which is related to the most distant BHs, agrees with the divergence point of the Joule-Thomson coefficient, which is depicted in a consistent manner [59, 60].

● We also presented the isenthalpic curves, and the results are presented in higher dimensions as can be observed in Figs. 15−18. It is very interesting to explain that the positive slopes of the inversion curve are found as mentioned in the literature [28, 56]. This indicates that with the expansion of a metric-affine universe, a BH always cools above the inversion curve.

● To determine the temperature gradients between the cooling and heating zones for various values of d_1, f_1, κ_{sh}, and κ_d, we analyzed the inversion curve (Figs. 19−22).

It is concluded that the considered BH in metric affine gravity agrees with the results in the literature. This work is beneficial for future research.

Declaration of competing interest

The authors declare that they have no known competing financial interests or personal relationships that could have appeared to influence the work reported in this paper.

Data Availability Statement

This manuscript has no associated data, or the data will not be deposited. (There is no observational data related to this article. The necessary calculations and graphic discussion can be made available on request.)

ACKNOWLEDGEMENTS

References

[1] R. Ruffini and J. A. Wheeler, Phys. Today **30**, 24 (1971)
[2] J. D. Bekenstein. arXiv: gr-qc/9808028
[3] J. D. Bekenstein, Phys. Rev. D **2333**, 8 (1973)
[4] S. W. Hawking, Commun. Eucl. Quant. Grav. 167 (1975)
[5] J. M. Bardeen, B. Carter, and S.W. Hawking, Commun. Math. Phys. **31**, 161 (1973)
[6] D. Kastor, S. Ray, and J. Traschen., Class. and Quant. Grav. **26**, 195011 (2009)
[7] Z. W. Feng *et al.*, The Eur. Phys. J. C **76**, 9 (2016)
[8] M. M. Caldarelli, G. Cognola, and D. Klemm, Class. Quant. Grav. **17**, 399 (2000)
[9] A. Chamblin, R. Emparan, C. V. Johnson *et al.*, Phys. Rev. D **60**, 064018 (1999)
[10] A. Chamblin, R. Emparan, C. V. Johnson and R .C. Myers, Phys. Rev. D **60**, 104026 (1999)
[11] B. P. Dolan, Class. Quant. Grav. **28**, 235017 (2011)
[12] D. Kubiznak and R. B. Mann, JHEP **07**, 033 (2012)
[13] D. Kubiznak, R. B. Mann, and M. Teo, Class. Quant. Grav. **34**, 063001 (2017)
[14] S. Gunasekaran, R. B. Mann, and D. Kubiznak, JHEP **11**, 110 (2012)
[15] A. Belhaj, M. Chabab, H. El Moumni *et al.*, Chin. Phys. Lett. **29**, 100401 (2012)
[16] S.H. Hendi and M.H. Vahidinia, Phys. Rev. D **88**, 084045 (2013)
[17] S. Chen, X. Liu, C. Liu *et al.*, Chin. Phys. Lett. **30**, 060401 (2013)
[18] E. Spallucci and A. Smailagic, Phys. Lett. B **723**, 436 (2013)
[19] R. Zhao *et al.*, Eur. Phys. J. C **73**, 2645 (2013)
[20] C. V. Johnson, Class. Quantum Grav. **31**, 205002 (2014)
[21] N. Altamirano, D. Kubiznak, and R. B. Mann, Phys. Rev. D **88**, 101502 (2013)
[22] H. H. Zhao *et al.*, Class. Quant. Grav. **32**, 145007 (2015)
[23] F. Javed *et al.*, Nucl. Phys. B **990**, 116180 (2023)
[24] F. Javed, Annals Phys. **458**, 169464 (2023)
[25] F. Javed, Eur. Phys. J. C **83**, 513 (2023)
[26] M. Sharif and F. Javed, Chin. J. Phys. **77**, 804 (2023)
[27] Ö. Ökcü and E. Aydiner, Eur. Phys. J. C **77**, 24 (2017)
[28] Ö. Ökcü and E. Aydiner, Eur. Phys. J. C **78**, 123 (2018)
[29] R. DAlmeida and K. P. Yogendran, arXiv: 1802.05116
[30] H. Ghaffarnejad, E. Yaraie, and M. Farsam, arXiv: 1802.08749
[31] M. Chabab *et al.*, arXiv: 1804.10042
[32] J. X. Mo *et al.*, arXiv: 1804.02650
[33] N. Dadhich and J. M. Pons, Gen. Rel. Grav. **44**, 2352 (2012)
[34] J. Beltran *et al.*, Phys. Rept. **727**, 129 (2018)
[35] V. I. Afonso *et al.*, Class. Quant. Grav. **34**, 235003 (2017)
[36] J. D. McCrea, Class. Quant. Grav. **9**, 553 (1992)
[37] B. Sebastian, J. Chevrier, and J. G. Valcarcel, J. Cosm. Astro. Part. Phys. **2023**, 018 (2023)
[38] F. W. Hehl *et al.*, Phys. Rept. **258**, 171 (1995)
[39] Y. Neueman and D. Sijacki, Annals Phys. **120**, 292 (1979)
[40] S. Bahamonde and J. Gigante Valcarcel, JCAP **09**, 057 (2020)

[41] H. Lenzen, Gen. Rel. Grav. **17**, 1137 (1985)
[42] C. M. Chen *et al*., Chin. J. Phys. **32**, 40 (1994)
[43] J. Ho, D. C. Chern and J. M. Nester, Chin. J. Phys **35**, 6 (1997)
[44] A. Campos and B. L. Hu, Int. J. Theor. Phys. **38**, 1271 (1999)
[45] B. L. Hu, A. Raval, and S. Sinha, arXiv: gr-qc/9901010
[46] S. Hyun and C. H. Nam, Eur. Phy. C **79**, 737 (2019)
[47] R. Maity, P. Roy, and T. Sarkar, Phys. Lett. B **765**, 386 (2017)
[48] A. Jawad and M. Shahzad, Eur. Phys. J. C **77**, 9 (2017)
[49] D. Allah *et al*., Phys. Dark Universe **77**, 9 (2017)
[50] S. W. Wei and Y. X. Liu, Nucl. Phys. B **946**, 114700 (2019)
[51] S. H. Hendi *et al*., Eur. Phys. C **75**, 457 (2015)
[52] M. Dehghani, Phys. Rev. D **97**, 044030 (2018)
[53] M. S. Ali and S. G. Ghosh, Phys. Rev. D **98**, 084025 (2018)
[54] S. Hawking and D. Page, Commun. Math. Phys. **87**, 577 (1983)
[55] P. Davis, Proc. R. Soc. A **353**, 499 (1977)
[56] A. Haldar and R. Biswas, EPL **123**, 40005 (2018)
[57] D. M. Yekta, A. Hadikhani, and Ö. Ökcü, Phys. Lett. B **795**, 527 (2019)
[58] S. Q. Lan, Phys. Rev. D **98**, 084014 (2018)
[59] H. Ghaffarnejad, E. Yaraie, and M. Farsam, Int. J. Theor. Phys. **57**, 1671 (2018)
[60] J. Pu *et al*., Chin. Phys. C **44**, 035102 (2020)
[61] S. I. Kruglov, Gravit. Cosmol. **29**, 57 (2023)
[62] Y.-Z. Du, X.-Y. Liu, Y. Zhang *et al*., Eur. Phys. J. C **83**, 426 (2023)
[63] M. Y. Zhang, H. Chen, H. Hassanabadi *et al*., Chin. Phys. C **47**, 045101 (2023)
[64] M. Chabab, H. El Moumni, S. Iraoui *et al*., arXiv: 1804.10042
[65] G. Yang, H. Xie, and Y.-G. Miao, Nucl. Phys. B 116280 (2023)
[66] S. Hui, B. Mu, and J. Tao, arXiv: 2207.01467